Supporting Information:

Efficient Coupling between Dielectric-Loaded Plasmonic and Silicon Photonic Waveguides

Ryan M. Briggs,[*,†] *Jonathan Grandidier,*[†] *Stanley P. Burgos,*[†] *Eyal Feigenbaum,*[†] *and Harry A. Atwater*[†,‡]

Thomas J. Watson Laboratories of Applied Physics, Kavli Nanoscience Institute, California Institute of Technology, Pasadena, California 91125

[*] To whom correspondence should be addressed, rbriggs@caltech.edu. [†] Thomas J. Watson Laboratories of Applied Physics. [‡] Kavli Nanoscience Institute.

Waveguide coupling setup: To couple light through grating-coupled silicon-on-insulator (SOI) waveguides, and subsequently through dielectric-loaded surface plasmon polariton (DLSPP) devices, we used a fiber-coupled New Focus 6428 Vidia Swept tunable diode laser source with identical input/output lensed fiber focusers,[1] as shown in Fig. S1. The pigtail focusers consist of single-mode fibers integrated with aspheric lens pairs designed for a 12.4-mm working distance and a spot size of approximately 10 μm. Between the laser and the input focuser, an in-line polarization controller was used to set the polarization at the input grating. From the output fiber, light was coupled into either a calibrated InGaAs power meter or a 10-MHz InGaAs

photoreceiver connected to a 500-MHz oscilloscope. The laser wavelength was swept linearly at a rate of 10 nm/s or slower for spectral measurements, resulting in sub-pm detector-limited wavelength resolution when using the photoreceiver.
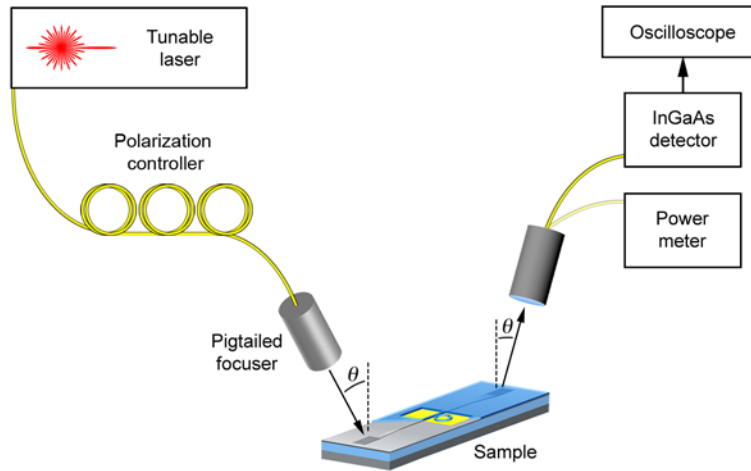
Figure S1. Schematic of the fiber-coupling setup used to couple light through SOI-waveguide-coupled DLSPP devices.

The lensed fiber focusers were mounted to rotation stages atop precision translation stages, allowing the focusers to be positioned above the SOI gratings and rotated eucentrically to access a specific grating coupling angle, θ. Positive coupling angles could be achieved with the configuration represented in Fig. S1, while negative coupling angles were accessible by focusing the input focuser onto the output grating, and vice versa. The long working distance of the fiber focusers allowed access to a relatively wide range of positive and negative coupling angles. Based on the overall transmission through our waveguide test setup and the input laser power, the grating-plus-taper loss is estimated to be 7 dB per coupler; however, we envision that with a waveguide-coupled on-chip light source, the devices we have developed could be realized

without free-space couplers. The insertion loss for DLSPP waveguides would then be just the SOI-DLSPP transition loss of approximately 1 dB.

Characterization of SOI waveguide modes: We analyzed the modes supported by our SOI waveguide geometry by investigating the response of a 400-μm diameter SOI ring resonator patterned on the same sample as the DLSPP ring devices. The ring was evanescently coupled to a straight SOI waveguide across a 1-μm gap.[1,2] In addition, the ring diameter is large enough that bending losses are negligible.[3] With a cross section identical to the SOI waveguides used for coupling light into the DLSPP waveguides, the SOI ring device supports just the fundamental transverse-electric (TE) and transverse-magnetic (TM) modes near $\lambda = 1550$ nm. By scanning the input wavelength through the straight waveguide, we observe coupling to whispering-gallery modes, as shown in Fig. S2. For diffraction-grating coupling angles of $\theta = +26°$ and $-26.5°$, we see coupling to either TE or TM resonator modes, respectively, confirming that the gratings allow for selective coupling to just one polarization due to the different phase velocities of the TE and TM modes. We can verify the identity of the whispering-gallery modes based on their free-spectral range, which is different for the two polarizations due to their unique group velocities.[1] Selective coupling to a single polarization proved useful for demonstrating that light is transmitted through the DLSPP waveguides only for the TM polarization.
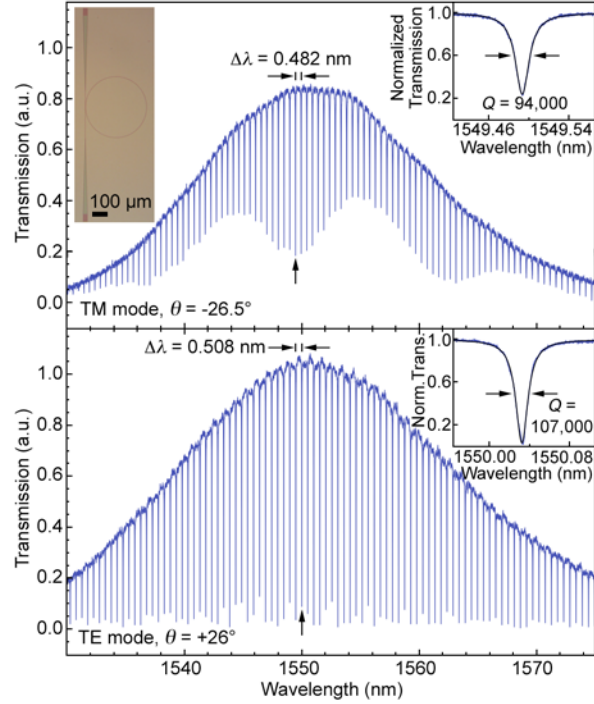
Figure S2. (Top panel) TM-mode transmission spectrum collected at a diffraction-grating coupling angle of θ = -26.5° for a waveguide coupled to a 400-µm diameter SOI ring resonator (shown in the optical micrograph). The inset shows a high-resolution wavelength scan at the indicated resonance along with the loaded quality factor obtained from a Lorentzian fit. The lower panel shows the transmission spectrum for the same device but with the light selectively coupled to the TE waveguide mode at a coupling angle of θ = +26°

As seen in the TM-mode transmission spectrum in the top panel of Fig. S2, obtained at a coupling angle of θ = -26.5°, the extinction ratio for the SOI ring-resonator whispering-gallery modes is largest near λ = 1550 nm, where the "magic-width" condition is satisfied.[4] The loaded resonator quality factor for the resonance centered near λ = 1549.5 nm is 94,000. By accounting for coupling loss, the intrinsic quality factor due to propagation loss, Q_{int}, can be determined.[2]

The high-resolution transmission spectrum, $T(\lambda)$, shown in the top inset of Fig. S2, was fit to the following form:[5]

$$T(\lambda) = \frac{(a-t)^2 + (2\pi n_g L_c)^2 \, at \, \dfrac{(\lambda - \lambda_0)^2}{\lambda_0^4}}{(1-at)^2 + (2\pi n_g L_c)^2 \, at \, \dfrac{(\lambda - \lambda_0)^2}{\lambda_0^4}}, \tag{S1}$$

which is derived from the general expression from Yariv[6] and is valid for small wavelength deviations around a central wavelength, λ_0. $L_c = 400\pi$ μm is the circumference of the SOI ring, n_g is the modal group index, and a and t account for attenuation due to propagation loss and coupling, respectively. The round-trip fractional loss, independent of coupling, is $l = -2 \ln(a)$, corresponding to an intrinsic quality factor of $Q_{int} = 2\pi n_g L_c/(\lambda_0 l) = 126{,}000$, where the group index, $n_g = 3.96$, can be obtained from the free-spectral range, $\Delta\lambda$, by the relation $n_g \approx \lambda_0^2/(\Delta\lambda L_c)$. The propagation loss is $-2 \ln(a)/L_c = 1.28$ cm^{-1}, or 5.5 dB/cm, which is more than two orders of magnitude lower than the DLSPP-waveguide loss at $\lambda = 1550$ nm.

The TE-mode transmission spectrum for the same device is shown in the lower panel of Fig. S2. The TE-polarized waveguide mode was accessed selectively using a coupling angle of $\theta = +26°$. The TE whispering-gallery modes are distinguishable from the TM modes because of their distinct free-spectral range, $\Delta\lambda$, and the absence of wavelength dependence in the extinction ratio. The TE-mode group index near $\lambda = 1550$ nm is 3.76, significantly smaller than the TM-mode group index. Accounting for coupling loss, the TE-mode propagation loss is 3.7 dB/cm.

Numerical simulations: We used COMSOL Multiphysics, a commercial finite-element method solver, to calculate the field distribution and complex effective index, n_{eff}, of the DLSPP waveguide modes. The real part of the effective index was accurately fit by a quadratic function

for wavelengths between $\lambda = 1500$ to 1600 nm. The fit was used in the interference model for the spectral response of the DLSPP ring resonators. Loss due to material absorption, α_{abs}, was determined from the imaginary part of the modal effective index as $\alpha_{abs} = 4\pi\, \text{Im}[n_{eff}]/\lambda$.

Mode calculations were performed using the Au index data measured by Johnson and Christy.[7] To obtain a continuous function for the real and imaginary parts of the index, we fit Hermite interpolation functions between the measured data points as well as between the reported error bars, as plotted in Fig. S3. The real and imaginary parts of the effective index that we report for the DLSPP waveguide mode between $\lambda = 1500$ to 1600 nm include the upper and lower limits within these interpolated errors.

Lumerical FDTD, a finite-difference time-domain solver, was used to model the coupling loss between DLSPP waveguides and SOI input/output waveguides. The built-in mode solver was used to define the SOI TM-mode source at $\lambda = 1550$ nm in the input waveguide, and the power flux was monitored in the SOI output waveguide 10 μm from the DLSPP-SOI output transition. The monitor position was varied to ensure that it captured only power coupled into the (loss-less) output waveguide and not power scattered from the DLSPP-SOI transitions. The simulation boundaries were defined as perfectly matched layers and positioned far enough away from the waveguide so as to minimally impact the effective index of the calculated input mode. To ensure stability, the input source was defined temporally as a single pulse, and the field amplitudes were allowed to decay to 0.001% of their initial values. Spectral filtering was used to extract the power transmission associated with the input wavelength.
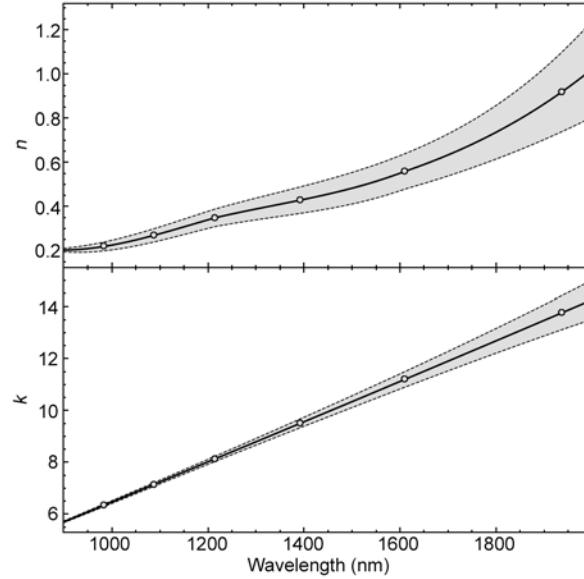
Figure S3. Real, *n*, and imaginary, *k*, parts of the index of refraction of Au used in the numerical calculations. The data points are from Ref. 7, and the curves are Hermite interpolations between the data points and their associated error bars.

Characterization of the waveguide geometry: The geometries of the SOI and DLSPP waveguides were verified using atomic-force microscopy (AFM). The AFM image in Fig. S4(a) shows the topography of an etched SOI ridge waveguide. A cross section from the image indicates that the waveguide width is close to the lithographically defined dimension of 740 nm, and the etch depth is 30 nm. Figure S4(b) shows the topography of a PMMA wire on Au from one of the SOI-waveguide-coupled DLSPP devices. The PMMA wire is nearly 500 nm wide at its top surface and approximately 560 nm tall. The AFM images of both the SOI and DLSPP waveguides were collected in non-contact mode, and the scanning parameters had to be carefully optimized to avoid damaging the soft, high aspect-ratio PMMA wires. The DLSPP waveguide geometry represented in Fig. S4(b) is consistent with measurements from electron micrographs of the patterned structures as well as film thickness measurements of unpatterned PMMA layers.
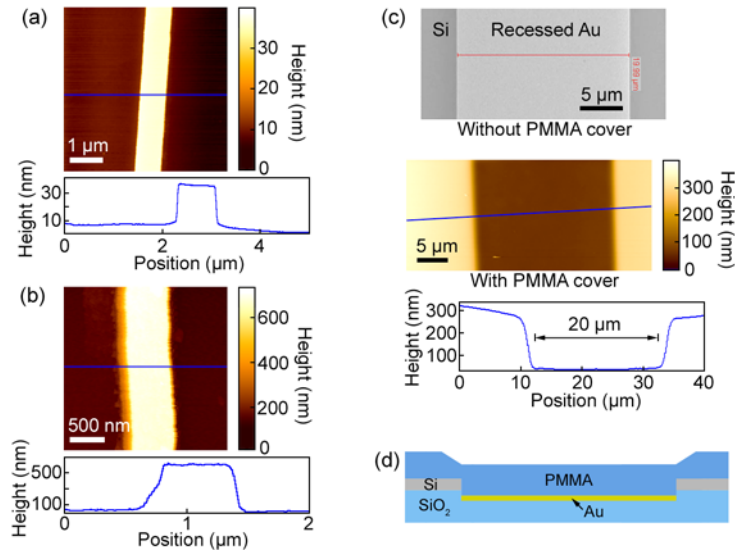
7

Figure S4. (a) AFM image of an etched SOI waveguide prior to coating with PMMA. A cross-section of the topography is shown in blue. (b) AFM image of a PMMA-on-Au DLSPP waveguide. (c) Scanning electron micrograph of a 20-μm wide recessed Au feature prior to coating with PMMA. The AFM image below the electron micrograph shows the topography of a feature of identical width after being coated with PMMA. The recessed region is 20 μm wide, indicating that the polymer coats the recessed Au with a uniform thickness. (d) A schematic cross-section of the PMMA-coated feature, showing that the polymer is tapered at the edges of the Si layer surrounding the Au region.

In order to accurately model the full three-dimensional structure of the SOI-waveguide-coupled DLSPP devices, we also used AFM to determine the topography of the spin-coated PMMA at the Si-Au interface. An essential feature of our waveguide design is the vertical offset of between the Si waveguiding layer and the Au surface that supports the DLSPP mode; however, this leads to varying topography on the top surface of the PMMA. The scanning

electron micrograph in Fig. S4(c) shows a recessed Au region on an SOI sample without a PMMA cover layer. The actual width of the recessed area is very close to the lithographically defined width of 20 μm. The contact-mode AFM image shows a feature fabricated in the same manner that has been subsequently coated with PMMA and baked at 180 °C for 5 min. We observe that the polymer conforms to the topography of the recessed structure, leading to a uniform height along the entire 20-μm wide recessed Au region. Furthermore, the vertical offset in the PMMA layer across the Si-Au interface is close to the 300-nm offset between the underlying Si and Au surfaces. From this analysis, we conclude that the PMMA uniformly covers the recessed Au, and there is an approximately 2-μm wide vertical taper in the polymer at the edges of the Si layer, as depicted schematically in Fig. S4(d).

NSOM measurements: To corroborate the surface plasmon propagation length obtained from variable-length waveguide transmission measurements, we analyzed the same DLSPP devices using near-field scanning optical microscopy (NSOM). NSOM/AFM measurements were performed with a tuning-fork based Nanonics MultiView 2000 scanning probe microscope in contact mode using a 200-nm diameter aperture probe in collection mode. Light was coupled into the SOI input waveguide of each device at a wavelength of 1520 nm using an identical lensed-fiber arrangement as used for the waveguide transmission measurements, and light collected by the scanning probe was detected using an InGaAs avalanche photodiode.

The NSOM analysis for a 30-μm long DLSPP waveguide is shown in Fig. S5. The AFM and NSOM images in Fig. S5(b) and (c) were collected simultaneously using a high gain setting for the tip deflection signal, which minimized damage to the polymer waveguide but led to a noticeable increase in the noise associated with the measured topography. Comparing the scanning electron micrograph in Fig. S5(a) with the AFM image in Fig. S5(b), we observe that

the size and shape of the NSOM tip affects the apparent width of the DLSPP waveguide in the x-direction; however, we are primarily interested in decay of the DLSPP mode along the propagation (z) direction. Consequently, we integrated the intensity in the NSOM image along the x-direction, which is plotted on a normalized logarithmic scale in Fig. S5(d) as a function of propagation distance along the z-direction. Other than an initial jump in intensity at the input SOI-DLSPP transition, the intensity decay resembles an exponential with a decay constant of approximately 50 µm. This is in agreement with the DLSPP-mode propagation length extracted from variable-length waveguide transmission measurements and therefore supports our quantitative analysis of the SOI-DLSPP waveguide coupling loss.

We observe significant intensity only along the polymer waveguide in the NSOM image, indicating that optical power is preferentially coupled into the DLSPP mode as opposed to air-Au surface plasmons, which would be expected to spread out from the sides of the waveguide. The beating in intensity along the propagation direction is attributed to interference between light in the DLSPP mode and light scattered into radiation modes at the SOI-DLSPP transitions. We note that oscillations of a similar period appear in the three-dimensional FDTD simulations of the coupled waveguide structure. Finally, we observe reduced intensity at the surface of the PMMA covering the SOI input/output waveguides because the SOI waveguide mode is largely confined to the buried Si layer.
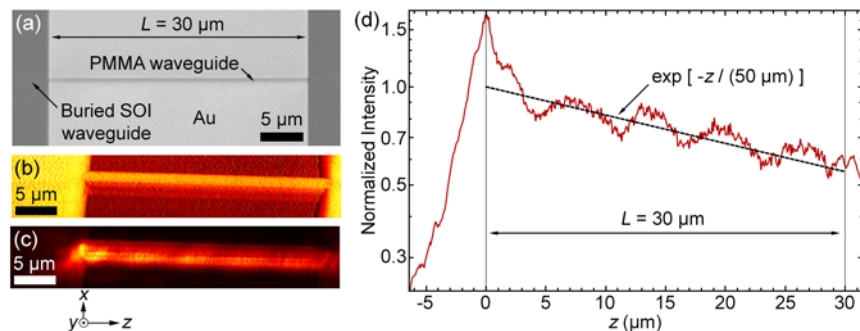

10

Figure S5. (a) Scanning electron micrograph of a 30-µm long DLSPP waveguide. (b) AFM and (c) NSOM images collected simultaneously for a device with the same geometry, where light was coupled into the plasmonic section from the buried SOI waveguide lying to the left of the DLSPP device. (d) Total collected intensity from the NSOM image integrated along the x-direction as a function of position in the propagation direction. The measured intensity exhibits a characteristic decay length of approximately 50 µm.

REFERENCES:

(1) Briggs, R. M.; Shearn, M.; Scherer, A.; Atwater, H. A. *Appl. Phys. Lett.* **2009**, *94*, 021106.

(2) Briggs, R. M.; Pryce, I. M.; Atwater, H. A. *Opt. Express* **2010**, *18*, 11192-11201.

(3) Marcuse, D. *IEEE J. Quantum Elect.* **1993**, *29*, 2957-2961.

(4) Webster, M. A.; Pafchek, R. M.; Mitchell, A.; Koch, T. L. *IEEE Photon. Technol. Lett.* **2007**, *19*, 426-431.

(5) Nitkowski, A.; Chen, L.; Lipson M. *Opt. Express* **2008**, *16*, 11930-11936.

(6) Yariv, A. *Electron. Lett.* **2000**, *36*, 321-322.

(7) Johnson, P. B.; Christy, R. W. *Phys. Rev. B* **1972**, *6*, 4370-4379.